


Measurement of the Low-Temperature Loss Tangent of High-Resistivity Silicon Using a High- Q Superconducting Resonator

M. Checchin[✉],* D. Frolov, A. Lunin, A. Grassellino, and A. Romanenko

Superconducting Quantum Materials and Systems Center, Fermi National Accelerator Laboratory, Batavia, Illinois 60510, USA

 (Received 5 November 2021; revised 16 June 2022; accepted 30 June 2022; published 7 September 2022; corrected 14 December 2022)

In this paper, we present a direct loss-tangent measurement of a high-resistivity intrinsic (100) silicon wafer in a temperature range from approximately 70 mK to 1 K, approaching the quantum regime. The measurement is performed using a technique that takes advantage of a high-quality-factor superconducting niobium resonator and allows us to directly measure the loss tangent of insulating materials with a high level of accuracy and precision. We report silicon-loss-tangent values at the lowest temperature and for electric field amplitudes comparable to those found in planar transmon devices, and these are one order of magnitude larger than what was previously estimated. In addition, we discover a nonmonotonic trend in the loss tangent as a function of temperature, which we describe by means of a phenomenological model based on variable-range hopping conduction between localized states around the Fermi energy. We also observe an increasing dependence of the dissipation on the electric field, which can be qualitatively described by the variable-range hopping-conduction mechanism as well. These findings are important for the optimization of quantum devices and for advancing the understanding of their decoherence channels.

DOI: [10.1103/PhysRevApplied.18.034013](https://doi.org/10.1103/PhysRevApplied.18.034013)

I. INTRODUCTION

Superconducting quantum circuits based on a cavity-quantum-electrodynamics architecture [1–3] represent a leading technology for constructing quantum processors and achieving quantum supremacy [4]. This technology utilizes the nanofabrication processes developed by the semiconductor industry to manufacture integrated microwave circuits. Silicon (Si) is a vital material in integrated-circuit technology and provides a good trade-off between losses in the millikelvin regime and process industrialization; therefore, it is the substrate of choice for superconducting-quantum-bit fabrication.

Because of the high dielectric constant of Si ($\epsilon'_r = 11.5$ at low temperatures), a large fraction of the electromagnetic energy in superconducting devices deposited on Si devices is stored in the silicon substrate [5]; hence, the contribution of this fraction to the overall energy loss in the device can be substantial. Accurate knowledge of the Si loss tangent is thus pivotal for correctly estimating dissipation in quantum devices.

High-resistivity silicon ($\rho \geq 5 \text{ k}\Omega \text{ cm}$) at millikelvin temperatures and microwave frequencies is generally assumed to introduce negligible dielectric losses compared with the native oxide and the substrate-metallization intermixing layers found in typical superconducting quantum devices. However, no direct measurements of Si-wafer loss tangents at millikelvin temperatures have been presented thus far. Therefore, a reasonably large degree of uncertainty in the actual value of the Si loss tangent in the millikelvin range still exists. Loss-tangent data for Si at millikelvin temperatures exist for silicon billets [6], which are not a representative sample of the wafers used to fabricate quantum bits, and for high-resistivity silicon at higher temperatures [7].

In this paper, we present a direct measurement of the loss tangent of high-resistivity floating-zone (FZ) silicon wafers in a temperature range from approximately 70 mK to 1 K. We discover a nonmonotonic trend in the loss tangent of silicon with temperature and an increasing trend in the dissipation with increasing electric field, which are inconsistent with known dissipation mechanisms encountered at these temperatures, such as two-level-system (TLS) absorption. Additionally, we demonstrate that the millikelvin Si loss tangent is one order of magnitude larger than previously estimated [8,9].

II. EXPERIMENTAL DETAILS

Measurements are performed using a high-quality-factor (Q -factor) elliptical superconducting niobium resonator

*Now at SLAC National Accelerator Laboratory, matyac@slac.stanford.edu

Published by the American Physical Society under the terms of the [Creative Commons Attribution 4.0 International](https://creativecommons.org/licenses/by/4.0/) license. Further distribution of this work must maintain attribution to the author(s) and the published article's title, journal citation, and DOI.

hosting a Si sample in the high-electric-field region. The fundamental mode TM_{010} , resonating at 2.6 GHz, is used to perform characterization of the sample over the entire temperature range.

Elliptical superconducting resonators operating at liquid-He temperatures are typically adopted in particle accelerators to accelerate relativistic charged particles because of their high efficiency (intrinsic Q -factor $Q_0 \sim 10^{11}$) in producing accelerating gradients on the order of tens of MV/m [10]. Nonetheless, they also allow $Q_0 \gtrsim 10^9$ at 10 mK [11], making them an ideal tool for performing loss-tangent measurements of insulators with a high degree of accuracy in the quantum regime.

Figure 1(a) shows a three-dimensional model of the experimental setup. The resonator is secured to the mixing-chamber plate of a dilution refrigerator (DR). The temperature is recorded by two ruthenium oxide (RuOx) thermometers, one attached to the mixing-chamber plate and one attached to the sample-holder transition flange, shown in green in Fig. 1(a)—the latter is referred to as the sample thermometer. The input line has several stages of attenuation with a total of approximately 60 dB, including Eccosorb filters. The output line has isolators and Eccosorb filters connected immediately after the device output port, and a 35-dB low-noise HEMT amplifier, which is thermalized with a quasi-4-K plate (typically stable at approximately 2.4 K). A simplified scheme of the microwave connections in the DR is shown in Fig. 1(b). The total gain of the transmitted-power line is measured to be approximately 62 dB, including a warm 40-dB amplifier [not shown in the schematic illustration in Fig. 1(b)].

Intrinsic FZ Si(100) single-side-polished wafers, with a thickness of 675 μm and a room-temperature resistivity of 10 k Ω cm, are procured and diced into strips 10 cm long

and 2 mm wide. After dicing, one sample is cleaned in an ultrasonic bath of isopropyl alcohol for 15 min, dried in ultrapure nitrogen, assembled onto the resonator, and subsequently pumped to a vacuum level of $p < 10^{-5}$ Torr.

The loaded Q -factor (Q_L) is measured with a power ring-down technique. A steady-state electromagnetic field is established in the resonator, and the free decay of the transmitted power (P_t) is recorded as a function of the time after shutting off the power fed to the device. The peak electric field in the Si sample in the steady state is measured to be approximately $E_{\text{Si}} = 5$ V/m, corresponding to an average number of photons stored in the resonator in the order of $\langle n \rangle \sim 5 \times 10^9$. This value is calculated by means of the proportionality factor $\kappa = E_{\text{Si}}/\sqrt{P_t Q_2} = E_{\text{Si}}/(\omega\sqrt{\hbar\langle n \rangle}) = 822$ V/(m W $^{1/2}$), obtained by finite-element simulations using the Ansys HFSS (high-frequency structure simulator) program, where Q_2 is the quality factor of the transmitted-line antenna [antenna 2 in Fig. 1(a)]. Note that, independently of the number of photons in the resonator, the maximum electric field experienced by the Si sample in this experiment is comparable to that induced by plasma oscillations in the Si substrates of typical transmon devices, which is found to be up to 20 V/m, corresponding to the metallization edges [12].

We define $Q_L = -10\omega/[(\ln 10)dP_t/dt]$, where ω denotes the angular frequency and dP_t/dt is the angular coefficient of the free decay of the transmitted power, with power measured in dBm. We then perform a linear regression to fit the decay data to extract dP_t/dt , selecting a window of points centered around 5 V/m. This strategy to measure Q_L is implemented to increase the measurement accuracy and circumvent the typical S21 measurement approach, which is limited by distortions of the resonant peak and the appearance of sidebands generated

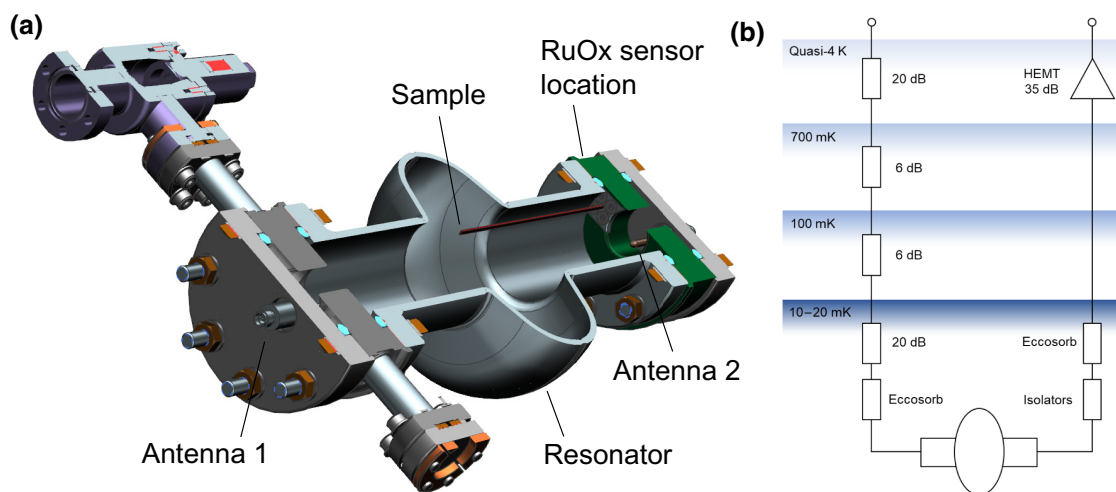


FIG. 1. Experimental setup. (a) Three-dimensional model of the experimental setup. (b) Schematic illustration of the experiment in the dilution refrigerator.

by microphonics [13] as a consequence of the high Q_L . Additional details regarding this measurement strategy are reported in Refs. [11,14].

III. RESULTS AND DISCUSSION

In Fig. 2, we illustrate the loaded Q -factor measured as a function of temperature. The blue dots represent the data for the loaded Q -factor (Q_L) acquired in this study, plotted against the sample temperature. The light blue diamonds show the intrinsic Q -factor of the resonator alone, without the Si sample, as measured in Ref. [11]. At thermal equilibrium, the sample can not be cooled below 74 mK due to a nonideal thermal path connecting the sample to the mixing chamber.

The loss tangent of the sample is calculated as follows:

$$\frac{1}{Q_S} = \frac{p_{\text{Si}}}{Q_{\text{Si}}} + \frac{p_{\text{SiO}_2}}{Q_{\text{SiO}_2}} = \frac{1}{Q_L} - \frac{1}{Q_0} - \frac{1}{Q_1} - \frac{1}{Q_2}, \quad (1)$$

where $Q_1 = 5.8 \times 10^9$ and $Q_2 = 6.5 \times 10^{11}$ represent the external Q -factors of the antennas [antenna 1 and antenna 2 in Fig. 1(a)] measured for the same setup in a liquid-helium bath at 1.5 K, as described in Ref. [15], and $p_{\text{Si}} = 9 \times 10^{-4}$ and $p_{\text{SiO}_2} = 3 \times 10^{-9}$ denote the participation ratios of silicon and the native silicon oxide layer, defined as follows: $p_{\text{diel}} = \int_{V_{\text{diel}}} \epsilon_{\text{diel}} |\mathbf{E}|^2 dV_{\text{diel}} / \int_V \epsilon_0 |\mathbf{E}|^2 dV$. Both values are calculated using the HFSS program.

It is important to highlight that the measured loaded Q -factor is dominated by the sample loss, whereas the other contributions are negligible. In fact, Q_0 is approximately 1

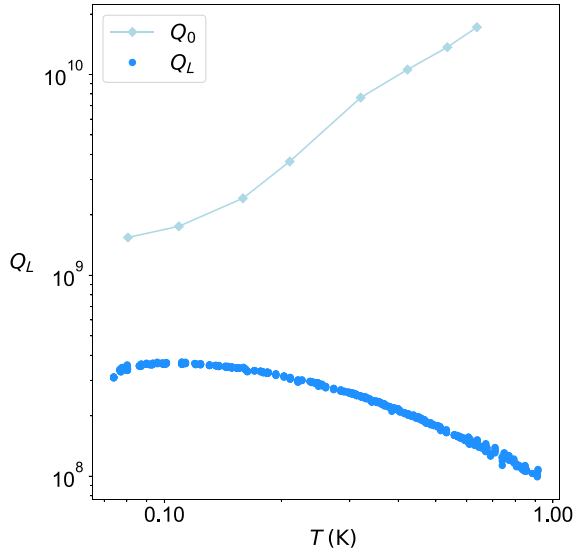


FIG. 2. The loaded quality factor as a function of the sample temperature is shown in blue. The resonator intrinsic Q -factor versus temperature at 2.6 GHz was reported in Ref. [11] and is shown in light blue.

order of magnitude higher than Q_L at the lowest temperature, while for temperature levels approaching 1 K, it is 2 orders of magnitude higher (see Fig. 2), and both Q_1 and Q_2 are at least 1 order of magnitude higher than Q_L . This implies that the measurement strategy implemented has a high level of accuracy and is not affected by dissipation mechanisms extrinsic to the sample under study.

The loss tangent of SiO_2 at millikelvin temperatures is experimentally known to be approximately $1/Q_{\text{SiO}_2} \simeq 5 \times 10^{-3}$ [16]. For the geometry under study, the participation ratio of the SiO_2 layer is calculated to be $p_{\text{SiO}_2} = 3 \times 10^{-9}$. Therefore, the SiO_2 contribution to Q_L is $Q_{\text{SiO}_2}/p_{\text{SiO}_2} \sim 10^{11}$, and hence is negligible compared with that of silicon. We can then define the silicon loss tangent as

$$\frac{1}{Q_{\text{Si}}} = \frac{1}{p_{\text{Si}} Q_S}. \quad (2)$$

Figure 3 shows the loss tangent of silicon as a function of the sample temperature. At the lowest temperature, 74 mK, the loss tangent is equal to 2.7×10^{-6} , which is in agreement with measurements performed on silicon billets in a whispering-gallery-mode configuration [6]. In contrast, our experiment records higher values compared with indirect estimations based on measurements and simulations of planar devices [8,9], which are in the order of 10^{-7} , one order of magnitude lower than our experimental observations.

We observe a nonmonotonic dependence of the silicon loss tangent on temperature, which does not resemble

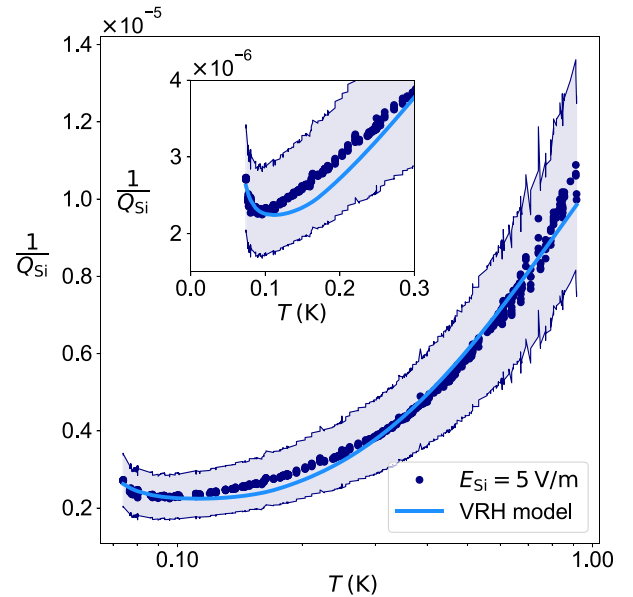


FIG. 3. Silicon loss tangent as a function of temperature. The blue solid line is a fit of the variable-range-hopping model to the experimental data. The shaded area represents the experimental error of the measurement. The inset is an enlargement of the data with temperature on a linear scale.

a TLS temperature dependence. The value of $1/Q_{\text{Si}}$ decreases with decreasing temperature, reaching a minimum at approximately 80 mK. Below 80 mK, the trend is opposite, and the loss tangent increases with a steeper slope as the temperature decreases. This trend can be better appreciated in the inset of Fig. 3, where the temperature is shown on a linear scale. The shaded areas show the experimental error associated with the measurement. This is calculated through error propagation, where the error in Q_L is propagated from the square root of the variance of the angular coefficient calculated by the linear-regression routine; the errors in Q_0 , Q_1 , and Q_2 are assumed to be 10%, while that in p_{Si} is estimated to be 25% and is calculated through HFSS simulations assuming a ± 2 -mm sample misalignment and $11.5 \leq \varepsilon_r \leq 11.9$.

To further shed light on the dissipation mechanism in place as a function of temperature, we calculate the electric field dependence of the loss tangent at constant temperature. We select three temperatures above, equal to, and below the minimum of the loss tangent as a function of T , nominally 74, 82, and 200 mK, and we calculate the silicon loss tangent by means of Eq. (1), where the loaded Q -factor is inversely proportional to the local slope of the transmitted-power ring-down data [$Q_L = -10\omega / [(\ln 10)dP_t/dt]$]. In Fig. 4, we show a parametric plot of the Si loss tangent versus the peak electric field E_{Si} . Interestingly, the electric field dependence of the loss

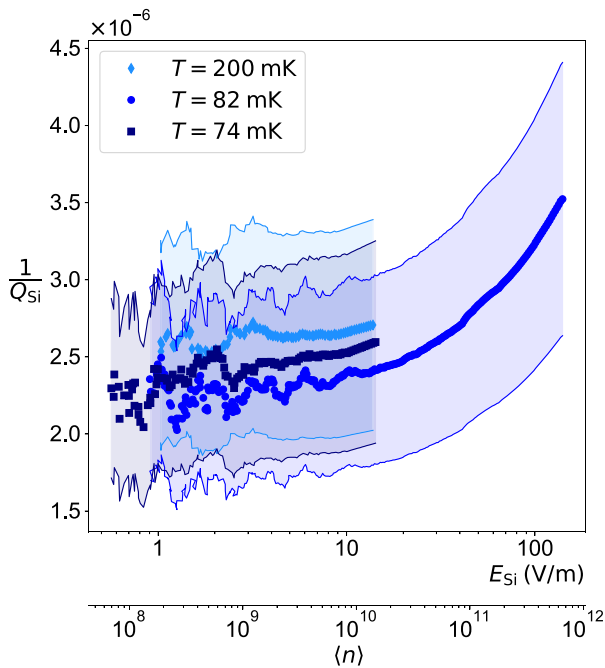


FIG. 4. Loss tangent as a function of the peak electric field in the sample, measured at fixed temperatures (74, 82, and 200 mK). The shaded areas represent the measurement error, estimated as discussed in the text. The second x axis shows the number of photons in the resonator.

tangent is also not in agreement with TLS-driven dissipation: $1/Q_{\text{Si}}$ decreases with decreasing field, and saturates at a constant value for $E_{\text{Si}} \lesssim 10$ V/m. The observed trend is independent of temperature—for temperatures above, equal to, and below the loss-tangent minimum, the field dependence is unchanged. This finding points against the possibility that the upward trend in $1/Q_{\text{Si}}$ for temperatures below 80 mK is due to TLS-type losses.

We exclude the possibility that the observed trend as a function of the electric field is due to an increase in the temperature of the sample because of thermal feedback. To prove this, we perform a series of free-decay experiments at a fixed temperature (82 mK) with increasing values of the input power (P_i); the experimental data are shown in Fig. 5. The thermalization time τ_T of the sample thermometer is observed to be roughly 2 min, while the loaded decay time τ_L of the resonator plus sample is measured to be in the order of 0.1 s. Since $\tau_L \ll \tau_T$, if any thermal feedback effect is at work then differences in the field dependence as a function of the steady-state P_i will be expected. On the contrary, the electric field dependence of the loss tangent is independent of the steady-state condition, suggesting that thermal feedback is negligible within the power range explored.

Based on our experimental findings, the source of dissipation should be sought in mechanisms that are not

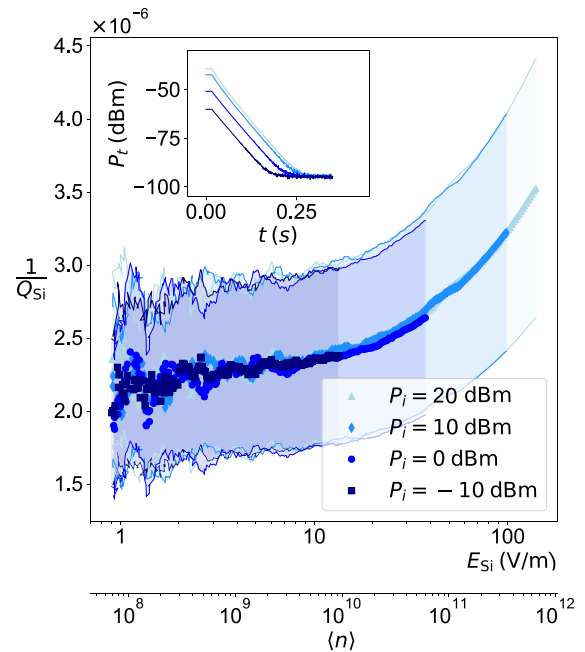


FIG. 5. Loss tangent as a function of the peak electric field in the sample, measured at 82 mK for different steady-state P_i values. The shaded areas represent the measurement error, estimated as discussed in the text. In the inset, we show the power-ring-down data as a function of time. The color palette of the data reported matches the colors of the main plot. The second x axis shows the number of photons in the resonator.

TLS-related. Rather, we expect that conduction losses could be the cause of the observed temperature and field dependences. Including conduction losses in the picture, the dielectric constant takes the form

$$\varepsilon = \varepsilon'_r - i \left(\varepsilon''_r + \frac{\sigma}{\omega \varepsilon_0} \right), \quad (3)$$

where ε'_r and ε''_r represent the real and imaginary parts, respectively, of the complex dielectric permittivity, and σ denotes the low-temperature conductivity. The loss tangent can then be expressed as follows:

$$\frac{1}{Q_{\text{Si}}} = \frac{1}{Q_{\text{TLS}}} + \frac{\sigma}{\omega \varepsilon_0 \varepsilon'_r}, \quad (4)$$

where the first term on the right-hand side, $1/Q_{\text{TLS}} = \varepsilon''_r/\varepsilon'_r$, denotes the dielectric loss tangent, dominated by dielectric dissipation (TLS), whereas the second term describes the conduction losses. Following the rationale discussed above, we can deem the TLS contribution of the Si oxide to be negligible.

We identify the dependence of the loss tangent on temperature with the second term of Eq. (4), and particularly with the occurrence of an electron-hopping mechanism, likely variable-range hopping (VRH) [17–19]. VRH conduction may take place at low temperatures, where localized states close to the Fermi level within approximately $\kappa_B T$ can contribute to the overall conduction. Electrons subjected to an electric field \mathbf{E} hop between states separated by the shortest four-dimensional distance, with three spatial coordinates and one energy coordinate, the so-called hopping range (\mathcal{R}), defined as

$$\mathcal{R} = 2\alpha R + \frac{W + e\mathbf{R} \cdot \mathbf{E}}{\kappa_B T},$$

$$W = \frac{3^4}{4^4 \pi g(\epsilon_F) R^3}, \quad (5)$$

where α , W , and R are the wave-function localization parameter, the average energy difference between the states [17,20], with $g(\epsilon_F)$ being the density of localized states within approximately $\kappa_B T$ around the Fermi energy ϵ_F , and the spatial distance between the states involved, respectively. The VRH conductivity can then be defined as being proportional to the difference between the hopping probabilities with and against the field \mathbf{E} , $\langle P^+ \rangle$ and $\langle P^- \rangle$:

$$\sigma_h \sim |\langle P^+ \rangle - \langle P^- \rangle| = \left| e^{-\min \mathcal{R}^+} - e^{-\min \mathcal{R}^-} \right|. \quad (6)$$

In the zero-field approximation, the distance R that minimizes \mathcal{R} in Eq. (5) always increases as the temperature is lowered, and conduction becomes dominated by hops between levels that are closer in energy even if they are far

apart, since the tunneling contribution [the first term on the right-hand side in the first line of Eq. (5)] becomes exponentially suppressed compared with the energy-activation term [the second term on the right-hand side in the first line of Eq. (5)]. In this approximation, the conductivity is expected to decrease approximately as $\exp(-T^{-1/4})$, and for $T \rightarrow 0$ it approaches zero exponentially [17,20].

In contrast, when $E > 0$, R increases at different rates depending on whether hops occur with or against the electric field, with the growth rate of R^- being larger. In turn, due to the $1/(R^-)^3$ dependence of W^- and the increasing weight of $-eR^-E$ that lowers the hopping activation energy, the VRH process is governed by \mathcal{R}^- , since this grows more slowly than \mathcal{R}^+ . As in the $E = 0$ case, σ_h decreases with decreasing T . However, if the temperature is lowered further, the condition $W^- < eR^-E$ is eventually met, and electron hopping against \mathbf{E} is not limited anymore by the activation energy. Consequently, the \mathcal{R}^- range reverses its trend and decreases with decreasing temperature, resulting in a sudden increase in σ_h (an increase in $\langle P^- \rangle$ and a decrease in $\langle P^+ \rangle$), and forms a minimum that eventually translates into a minimum of $1/Q_{\text{Si}}$ versus T .

We fit the experimental data as a function of temperature by means of a phenomenological model based on the VRH mechanism described above. We rewrite Eq. (4) assuming two conduction-loss channels, specifically VRH (defined by σ_h) and a residual term (defined by σ_0) that allows a better fit outcome. Equation (4) is rewritten as

$$\frac{1}{Q_{\text{Si}}} = \frac{\sigma_h + \sigma_0}{\omega \varepsilon_0 \varepsilon'_r}, \quad (7)$$

where the hopping conductivity is calculated as

$$\sigma_h = \frac{|J^+ - J^-|}{E}, \quad (8)$$

and where $J = 2e\gamma g(\epsilon_F)\kappa_B T R \langle P \rangle$ and γ is the hopping attempt frequency [17,20].

A least-squares regression routine is run by numerically calculating the values R^+ and R^- that minimize \mathcal{R}^+ and \mathcal{R}^- , respectively, keeping α , γ , $g(\epsilon_F)$, and σ_0 as free parameters. The fit is reported in Fig. 3. As shown, the model describes the data exhaustively within the experimental error, returning the following values: $\alpha^{-1} = 1.05 \mu\text{m}$, $\gamma = 11.4 \text{ THz}$, $g(\epsilon_F) = 1.33 \times 10^{13} \text{ eV}^{-1} \text{ cm}^{-3}$, and $\sigma_0 = 0.52 \mu\text{S/m}$. We interpret the σ_0 contribution as a manifestation of the excitation of free carriers in the conduction band, likely generated by cosmic ray absorption—due to the large dimensions of the sample, a non-negligible fraction of excitations in the conduction band is expected. Because of the lack of literature on VRH in high-resistivity intrinsic silicon, we compare the values returned by the fitting routine with values for amorphous silicon. The γ value obtained falls within the range $\gamma \approx$

(3–15) THz reported in Ref. [21], while $g(\epsilon_F)$ and α are smaller than what are reported for amorphous silicon, where $g(\epsilon_F) \simeq (10^{16}–10^{23}) \text{ eV}^{-1} \text{ cm}^{-3}$ and $\alpha^{-1} \simeq (0.1–10) \text{ nm}$ [21,22]. These findings imply (i) that, as expected, the number of available states in high-resistivity intrinsic silicon is less and they are separated by a larger distance compared with amorphous silicon, and (ii) that the states involved in the hopping-conduction mechanism are not well localized.

The VRH mechanism can qualitatively describe the experimental data as a function of the electric field as well, and for low E values the conductivity is expected to increase with the field as $\sigma_h \sim \sinh(eRE/\kappa_B T)$ [20]. However, the fitting routine does not interpolate the data exhaustively, suggesting that a generalized first-principles theoretical model is needed to describe accurately the field dependence observed. Nevertheless, the model presented here provides insights into the suspected loss mechanism at play at millikelvin temperatures.

IV. CONCLUSIONS

In summary, we report a direct measurement of the loss tangent of a high-resistivity silicon wafer in a temperature range from approximately 70 mK to 1 K. We show that the loss tangent of high-resistivity Si in the millikelvin range is one order of magnitude higher than that previously estimated indirectly from measurements and simulations of planar devices [8,9], although it is in agreement with values obtained from whispering-gallery measurements on Si billets [6]. In addition, we discover a nonmonotonic behavior of the dependence of the loss tangent on temperature with a minimum at approximately 80 mK, which we interpret as the occurrence of a change in the sign of the slope of the against-field hopping range (\mathcal{R}^-) as a function of temperature. We also observe a decreasing trend in the loss tangent with decreasing electric field, with saturation below approximately 10 V/m, which can be described only qualitatively by the VRH mechanism. More experimental studies are under way to fully characterize the dissipation in silicon in the millikelvin regime and uncover the detailed nature of the underlying mechanisms at play.

The methodology developed in this study will serve as a tool for detailed investigations of losses in dielectrics at millikelvin temperatures, and guide the selection of materials for the fabrication of high-coherence quantum devices.

ACKNOWLEDGMENTS

This paper is based on work supported by the U.S. Department of Energy, Office of Science, National Quantum Information Science Research Centers, Superconducting Quantum Materials and Systems Center (SQMS) under Contract No. DE-AC02-07CH11359.

- [1] A. Wallraf, D. I. Schuster, A. Blais, L. Frunzio, R.-S. Huang, J. Majer, S. Kumar, S. M. Girvin, and R. J. Schoelkopf, Strong coupling of a single photon to a superconducting qubit using circuit quantum electrodynamics, *Nature* **431**, 162 (2004).
- [2] R. J. Schoelkopf and S. M. Girvin, Wiring up quantum systems, *Nature* **451**, 664 (2008).
- [3] M. H. Devoret and R. J. Schoelkopf, Superconducting circuit for quantum information: An outlook, *Science* **339**, 1169 (2013).
- [4] F. Arute, K. Arya, R. Babbush, D. Bacon, J. C. Bardin, R. Barends, R. Biswas, S. Boixo, F. G. S. L. Brandao, and D. A. Buell, *et al.*, Quantum supremacy using a programmable superconducting processor, *Nature* **574**, 505 (2019).
- [5] C. Wang, C. Axline, Y. Y. Gao, T. Brecht, Y. Chu, L. Frunzio, M. H. Devoret, and R. J. Schoelkopf, Surface participation ratio and dielectric loss in superconducting qubits, *Appl. Phys. Lett.* **107**, 162601 (2015).
- [6] J. Bourhill, M. Goryachev, D. L. Creedon, B. C. Johnson, D. N. Jamieson, and M. E. Tobar, Low-temperature properties of whispering-gallery modes in isotopically pure silicon-28, *Phys. Rev. Appl.* **11**, 044044 (2019).
- [7] J. Krupka, J. Breeze, A. Centeno, N. Alford, T. Claussen, and L. Jensen, Measurements of permittivity, dielectric loss tangent, and resistivity of float-zone silicon at microwave frequencies, *IEEE Trans. Microw. Theory Tech.* **54**, 3995 (2006).
- [8] W. Woods, G. Calusine, A. Melville, A. Sevi, E. Golden, D. K. Kim, D. Rosenberg, J. L. Yoder, and W. D. Oliver, Determining interface dielectric losses in superconducting coplanar-waveguide resonators, *Phys. Rev. Appl.* **12**, 014012 (2019).
- [9] A. Melville, G. Calusine, W. Woods, K. Serniak, E. Golden, B. M. Niedzielski, D. K. Kim, A. Sevi, J. L. Yoder, E. A. Dauler, and W. D. Oliver, Comparison of dielectric loss in titanium nitride and aluminum superconducting resonators, *Appl. Phys. Lett.* **117**, 124004 (2020).
- [10] A. Romanenko, A. Grassellino, A. C. Crawford, D. A. Sergatskov, and O. Melnychuk, Ultra-high quality factors in superconducting niobium cavities in ambient magnetic fields up to 190 mG, *Appl. Phys. Lett.* **105**, 234103 (2014).
- [11] A. Romanenko, R. Pilipenko, S. Zorzetti, D. Frolov, M. Awida, S. Belomestnykh, S. Posen, and A. Grassellino, Three-dimensional superconducting resonators at $T < 20 \text{ mK}$ with photon lifetimes up to $\tau = 2 \text{ s}$, *Phys. Rev. Appl.* **13**, 034032 (2020).
- [12] J. Lisenfeld, A. Bilmes, A. Megrant, R. Barends, J. Kelly, P. Klimov, G. Weiss, J. M. Martinis, and A. V. Ustinov, Electric field spectroscopy of material defects in transmon qubits, *Npj Quantum Inf.* **5**, 105 (2019).
- [13] H. Padamsee, J. Knobloch, and T. Hays, *RF Superconductivity for Accelerators* (Wiley-VCH Verlag GmbH and Co., KGaA, Weinheim, 2008).
- [14] A. Romanenko and D. I. Schuster, Understanding quality factor degradation in superconducting niobium cavities at low microwave field amplitudes, *Phys. Rev. Lett.* **119**, 264801 (2017).
- [15] O. Melnychuk, A. Grassellino, and A. Romanenko, Error analysis for intrinsic quality factor measurement

- in superconducting radio frequency resonators, *Rev. Sci. Instrum.* **85**, 124705 (2014).
- [16] J. M. Martinis, K. B. Cooper, R. McDermott, M. Steffen, M. Ansmann, K. D. Osborn, K. Cicak, S. Oh, D. P. Pappas, R. W. Simmonds, and C. C. Yu, Decoherence in Josephson qubits from dielectric loss, *Phys. Rev. Lett.* **95**, 210503 (2005).
- [17] N. F. Mott, Conduction in glasses containing transition metal ions, *J. Non-Cryst. Solids* **1**, 1 (1968).
- [18] N. Apsley and H. P. Hughes, Temperature- and field-dependence of hopping conduction in disordered systems, *Philos. Mag.* **30**, 963 (1974).
- [19] N. Apsley and H. P. Hughes, Temperature- and field-dependence of hopping conduction in disordered systems, II, *Philos. Mag.* **31**, 1327 (1975).
- [20] N. F. Mott and E. A. Davis, *Electronic Processes in Non-Crystalline Solids* (Oxford University Press Inc., New York, 1979).
- [21] R. Pfeilsticker, S. Kalbitzer, and G. Müller, Observation of variable range hopping at “natural” phonon frequencies, *Z. Phys. B* **31**, 233 (1978).
- [22] L. Pichon and R. Rogel, Experimental validation of the exponential localized states distribution in the variable range hopping mechanism in disordered silicon films, *Appl. Phys. Lett.* **99**, 072106 (2011).

Correction: The math terms in the HTML version were processed incorrectly in the production process and have been rendered properly now.